

Maximal electric power generation from varying ocean waves with LC-tuned reactive PTO force

Jingxin Zhang¹, Uzair Bin Tahir¹, and Richard Manasseh¹

¹Affiliation not available

April 26, 2024

Maximal electric power generation from varying ocean waves with LC-tuned reactive PTO force

Jingxin Zhang*, Uzair Bin Tahir*, Richard Manasseh

Abstract—The reactive Power Take Off (PTO) force is the key to maximizing mechanical power absorption and electric power generation of Wave Energy Converters (WECs) from ocean waves with variable frequency, but its study is limited due to its difficulty in physical realization. This paper presents a simple yet effective LC-tuned WEC that generates a tunable reactive PTO force from tunable inductor L and capacitor C in the WEC. A complete closed loop system model of the WEC is derived first, then three quantitative rules are obtained from analyzing the model. These rules are used to tune the LC network, and hence the reactive PTO force that drives the WEC, to resonate with the input wave force and generate maximal electric power over a range of wave frequencies. Mathematical analysis of the WEC and tuning rules reveals the analytical and quantitative descriptions of the WEC’s mechanical power absorption, active and reactive electric power generation and power factor, optimal electric resistance load, and the generator and LC capacity requirements. Simulation results show the effectiveness and advantages of the proposed WEC and verify the analysis results.

Index Terms—WEC, reactive generator current, reactive PTO force, mechanical power absorption, electric power generation.

I. INTRODUCTION

WAVE energy converters (WECs) play the central role in ocean wave power generation, converting wave energy to electric energy. Among various types of WECs, the point absorber WEC is one of the simplest and most promising types [1] and is the WEC addressed in this paper.

A WEC absorbs more power to produce electricity when it resonates with incoming waves. But this is extremely difficult to sustain under varying waves and electric loads [1]–[3]. To solve this problem, the power take off (PTO) system of the WEC is used to maximize power absorption in such situations.

The PTO system is a crucial part of a WEC. It absorbs mechanical power from the WEC’s oscillator, generates the PTO force against the wave input force to sustain oscillation and mechanical power absorption, and converts absorbed mechanical power to electric power with the WEC’s generator. Its design and operation directly affect the mechanical power absorption and electric power generation of the WEC [4].

In attempts to make a WEC resonate over a range of frequencies around its natural frequency, many mechanical PTO methods have been proposed in the literature that can ‘tune’ the WEC, e.g., hydraulic PTOs [5], reactive actuators [6], auxiliary mass control [7], impedance matching [8], latching control [9], geometry and position control [10] and

conventional spring-damper systems [11]. These methods do not address electric power generation directly, and generally require additional mechanical and electrical devices and external power injection, on top of the generator and wave input power, to generate and control the PTO force. Hence, they tend to be complex, expensive, inefficient and less responsive, and may lower the net (electric) power output of the WEC.

In attempts to directly maximize the WEC’s electric power generation under varying waves, many electrical PTO methods have also been proposed, e.g., electric resistive latching [12], impedance tuning [13], damping control [14], reactive control [15], and maximum power point tracking [16], [17]. These methods use the WEC’s generator to generate and control the PTO force while producing electricity, without additional devices and external power injection. Thus, they are simpler, lower cost, more responsive and efficient, and may maximize the net (electric) power output of the WEC.

Despite their advantages, the electrical methods share a common problem: they only focus on the generation of active electric power and overlook the reactive electric power required by such generation. Many of them use the d-q axis generator model and intentionally zero or suppress one axis current to block or minimize the generator’s reactive current, e.g., [12], [14], [18]. As a result, they generally do not produce reactive PTO forces. As shown in some previous works [3], [6]–[8], [19] and also in the sequel, the reactive PTO forces are the key to making the WEC resonate and hence to maximizing electric power generation over a range of wave frequencies. The lack of reactive PTO forces makes it difficult for the electrical methods to maximize electric power generation and may result in the negative electric power generation observed in [18] and references therein. Overlooking the generator’s reactive current has also led to the absence of device sizing analyses, e.g. an analysis of generator capacity rating, in the existing works.

To solve these problems, we propose a new WEC structure with a novel electric PTO system comprising a permanent magnet linear generator (PMLG) in parallel connection with tuneable inductor L and capacitor C , as shown in Fig. 1. The L and C are used to produce respectively the lagging and leading reactive currents in the generator to induce the lagging and leading reactive PTO forces vs the wave input force. By tuning the L and C and hence the reactive PTO forces according to the wave frequency, we keep the WEC resonating and its active electric power output constant and maximal over a range of wave frequencies, under ideal conditions.

To reveal the underlying physics of the proposed WEC, we use the ideal models of 1D ocean waves and linear WECs, and a simplified single phase linear generator with negligible internal resistance and inductance in our derivation

This work was funded by ACSRF-WWE and performed at Swinburne University of Technology, Australia.

J. Zhang and U. Tahir (*equal first authors) are with the School of Science, Computing and Engineering Technologies, Swinburne University of Technology, 3122, Victoria, Australia (jingxinzhang, utahir@swin.edu.au).

R. Manasseh is with the School of Engineering, Swinburne University of Technology, 3122, Victoria, Australia (rmanasseh@swin.edu.au).

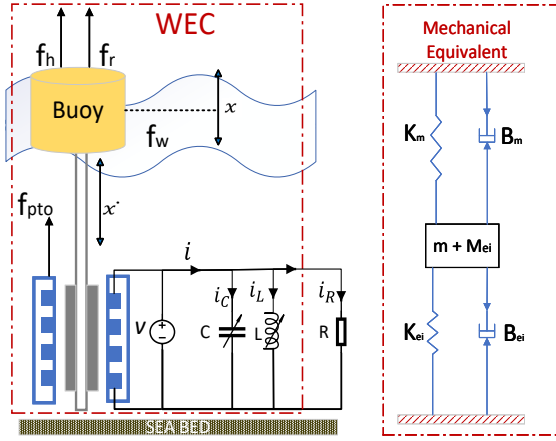


Fig. 1. New WEC structure and mechanical-electrical interaction model

and analysis. Also, we only consider steady state operation of the WEC without dynamic control of the PTO. The proposed setup allows the derivation of a complete closed loop system model of the proposed WEC, quantitative and analytical descriptions and conditions for maximum mechanical absorption, maximum active electric power generation, the active, reactive and apparent powers and power factor of the WEC's generator, and generator capacity rating in term of apparent power. All of these are previously unknown results to the best of our knowledge.

The rest of paper is organized as follows. Section II describes the proposed new WEC, its PTO force, and its closed loop system model. Section III presents the LC tuning rules of the new WEC, and the quantitative analysis and analytical results of these rules. Section IV presents a simulation verification and demonstration of the analytical results. Section V draws the conclusions and discusses the implications, limitations and extensions of the presented results.

II. PROPOSED NEW WEC STRUCTURE AND MODEL

A. Proposed new WEC structure

Fig. 1 (left) shows our proposed new WEC structure. It has a heaving buoy driven by the ocean waves and connected to the PMLG by a shaft. The PMLG is connected to a tunable parallel LC network that provides electricity to the load (resistor) R . This structure is similar to the class of WECs using direct electric drive as the PTO system [20], but its tunable LC network and PMLG form a new type of PTO system that can be tuned to maximize the electric power output to the load R over a range of wave frequencies. Though simple, the basic principle derived from the proposed WEC is applicable to other classes of WECs [1], [2], [21], as long as their mechanical operation can be modelled as a resonating linear mass-damper-spring system.

Fig. 1 (right) shows the Mechanical-Electrical (M-E) interactions in the proposed WEC. As the buoy oscillates, it moves the PMLG's translator to generate the voltage $v(t)$ that drives the current $i(t)$ through the RLC network; the current $i(t) = i_R(t) + i_L(t) + i_C(t)$, in turn, induces the electrical resistive force $f_{pto}(t) = f_R(t) + f_L(t) + f_C(t)$ with three sub-forces on the shaft of the PMLG; the three sub-forces exerted

through the shaft to the buoy induce the equivalent mass M_{ei} , damping B_{ei} and stiffness K_{ei} that affect the overall system dynamics. It is assumed that the input wave frequency may vary; typically, ocean swell waves with periods $\mathcal{O}(1 - 10 \text{ s})$, which carry the most energy, vary over timescales of days [22]. However, the wave frequency is assumed to be known, and the LC network is tuned, in accordance with the wave frequency, to control the current $i(t)$ and hence the $f_{pto}(t)$ to achieve resonance at different wave frequencies.

B. Open loop dynamic model of proposed WEC

To reveal the fundamental M-E dynamics, we assume that the whole WEC system is linear, the water is homogeneous, inviscid, irrotational and incompressible and the waves are sinusoidal, so the waves are describable by potential-flow theory [1], [3]; the added mass corresponding to the radiation force is constant [17], [23]; the shaft is rigid and lossless, and hence the buoy and translator (BT) and its added fluid mass move together as a single mass and all the masses are lumped into the system total mass M_m . These assumptions encapsulate the essential traits of WECs and are commonly employed in the analysis and design of WECs [24], [25].

Denote $x(t)$, $\dot{x}(t)$ and $\ddot{x}(t)$ the displacement, velocity and acceleration of the BT, respectively. Then, by the linear potential theory and Newton's second law of motion, the dynamics of the proposed WEC can be described, as commonly formulated [25], [26] by

$$M_m \ddot{x}(t) = f_w(t) - f_{pto}(t) - f_r(t) - f_h(t), \quad (1)$$

where $f_w(t)$ is the wave excitation force, $f_r(t)$ the radiation force, $f_h(t)$ the hydrostatic stiffness force, and $f_{pto}(t)$ the resistive force from the PTO system of proposed WEC.

As often assumed in fundamental linear analyses of WECs [24], the excitation force $f_w(t)$ is from regular incident waves, with angular wave frequency ω , constant amplitude A_w and no phase difference, and takes the form

$$f_w(t) = A_w \cos(\omega t). \quad (2)$$

It is well known that A_w is proportional to the total mass M_m , the larger the M_m , the higher the A_w [1]. The radiation force $f_r(t)$ (the fluid force due to the oscillating body) is approximated by Cummins' equation [27] as

$$f_r(t) = B_m \dot{x}(t), \quad (3)$$

where B_m is the radiation damping constant due to the interaction of the buoy motion and surrounding water.

The hydrostatic stiffness force $f_h(t)$ is described as [23], [28]

$$f_h(t) = K_m x(t), \quad (4)$$

where $K_m = \rho g S$ is the hydrostatic stiffness, with ρ the water density, g the acceleration due to gravity and S the cross-sectional area of buoy.

With the $f_r(t)$ and $f_h(t)$ given above, the hydrodynamic equation (1) of the WEC can be written as

$$M_m \ddot{x}(t) + B_m \dot{x}(t) + K_m x(t) = f_w(t) - f_{pto}(t), \quad (5)$$

where $f_r(t) = B_m \dot{x}(t)$ and $f_h(t) = K_m x(t)$ are moved to the left hand side since they are the feedback forces induced by $\dot{x}(t)$ and $x(t)$, while $f_w(t)$ and $f_{pto}(t)$ are kept on the right since $f_w(t)$ is an independent external force from waves, and the nature of $f_{pto}(t)$ is unknown and to be analyzed.

C. Analysis of $f_{pto}(t)$ and closed loop dynamic model of proposed WEC

To analyze the $f_{pto}(t)$ force of the proposed WEC system, we assume the PMLG in Fig 1 (left) is a 1-phase machine with $N_p = 2$ poles that generates a sinusoidal output voltage when its translator is in steady reciprocal motion. Examples of such PMLGs can be found in [29] and the references therein. Since the internal resistance R_{in} and inductance L_{in} of a generator are generally much smaller than the external load R and L [30], we neglect R_{in} and L_{in} to simplify discussion without loss of essence. Hence, the PMLG's internal voltage $v(t)$ equals its terminal output voltage and the oscillation of $v(t)$ follows that of the translator, with the same frequency.

By electrical machine theory [30], when the PMLG's translator moves at the velocity $\dot{x}(t)$, driven by the input force $f_w(t)$, an internal voltage $v(t)$ is induced in its stator winding, with

$$v(t) = K_e \dot{x}(t), \quad (6)$$

where K_e is the electric constant. The internal voltage $v(t)$ then drives a current $i(t)$ through the PMLG and the RLC network. The current $i(t) = i_R(t) + i_L(t) + i_C(t)$, in turn, induces a resistive force comprising three components on the translator shaft,

$$f_{ei}(t) = K_t i(t) = K_t i_R(t) + K_t i_L(t) + K_t i_C(t) \quad (7)$$

where K_t is the force constant satisfying $K_t = K_e$, although their physical units are different [30].

Using (6), $i_R(t) = v(t)/R$, $i_L(t) = \frac{1}{L} \int v(t) dt$ and $i_C(t) = C dv(t)/dt$, the RLC currents can be written as

$$i_R(t) = \frac{K_e \dot{x}(t)}{R}, \quad i_L(t) = \frac{K_e}{L} x(t), \quad i_C(t) = C K_e \ddot{x}(t). \quad (8)$$

Define the electrically induced mass, damping and stiffness

$$M_{ei} := K_t K_e C, \quad B_{ei} := K_t K_e / R, \quad K_{ei} := K_t K_e / L. \quad (9)$$

Then by (6)-(9), the electrically induced resistive force $f_{ei}(t)$ and its three sub-forces can be written as

$$f_{ei}(t) = K_t i(t) = M_{ei} \ddot{x}(t) + B_{ei} \dot{x}(t) + K_{ei} x(t) \quad (10)$$

$$f_C(t) := K_t i_C(t) = M_{ei} \ddot{x}(t), \quad (\text{reactive leading}) \quad (11)$$

$$f_R(t) := K_t i_R(t) = B_{ei} \dot{x}(t), \quad (\text{active}) \quad (12)$$

$$f_L(t) := K_t i_L(t) = K_{ei} x(t). \quad (\text{reactive lagging}) \quad (13)$$

As shown in Section III, $f_R(t)$ is the active sub-force; $f_C(t)$ and $f_L(t)$ are respectively the reactive leading and lagging sub-forces absorbing zero average mechanical power.

Since $f_{ei}(t)$ is the only force from the PMLG against the input force $f_w(t)$, $f_{ei}(t) = f_{pto}(t)$ in (5). Substituting (10) into (5) gives the closed-loop dynamic model of the proposed WEC

$$(M_m + M_{ei}) \ddot{x}(t) + (B_m + B_{ei}) \dot{x}(t) + (K_m + K_{ei}) x(t) = f_w(t). \quad (14)$$

As shown below, (14) is a passive linear system with bounded input and bounded output (BIBO) stability and hence admits the Fourier transform (on both sides) [31]

$$[(j\omega)^2(M_m + M_{ei}) + j\omega(B_m + B_{ei}) + (K_m + K_{ei})] X(j\omega) = F_w(j\omega). \quad (15)$$

Rearranging (15) and defining the frequency response function

$$H(j\omega) := \frac{1}{(K_m + K_{ei}) - \omega^2(M_m + M_{ei}) + j\omega(B_m + B_{ei})} \quad (16)$$

gives the input-output frequency response model of the proposed WEC system

$$X(j\omega) = H(j\omega) F_w(j\omega). \quad (17)$$

As seen from (5), (10), (14) and (17), the proposed WEC is a closed loop system, with a single input $f_w(t)$ ($F_w(j\omega)$ in the frequency domain), a single output $x(t)$ ($X(j\omega)$), and the closed loop frequency response function $H(j\omega)$. As a single-input-single-output system, $f_w(t)$ ($F_w(j\omega)$) is the only source of (mechanical) energy input. The feedback loop is closed by the feedback force $f_{pto}(t) = f_{ei}(t) = f_C(t) + f_R(t) + f_L(t)$, with all three sub-forces internally generated by the PMLG and RLC network using only the mechanical input energy. Hence, the energy of the output $x(t)$ ($X(j\omega)$) is always less than or equal to the energy of the input $f_w(t)$ ($F_w(j\omega)$). As the input energy from $f_w(t)$ ($F_w(j\omega)$) is always bounded (finite), so is the output energy of $x(t)$ ($X(j\omega)$). By signals and systems theory [31], (14) ((17)) is a passive linear system with BIBO stability.

Remark 1: The force $f_{ei}(t) = f_{pto}(t)$ given in (10) is in the same form of the general linear PTO (GLPTO) force, $f_{pto}(t) = M_{pto} \ddot{x}(t) + B_{pto} \dot{x}(t) + K_{pto} x(t)$, implicitly and conceptually proposed in [6], [17]. However, the GLPTO has been utilized mainly in models where the intent is maximizing the mechanical power absorption of WECs from ocean waves, but not for maximal electrical power generation. As a result, the conceptual GLPTO generally involves additional mechanical and electrical devices that are not used for electric power generation and need external power injection (negative power flow) for their operation. Also, the GLPTO is mostly conceptual. To the best of our knowledge, there has been no physical realization of GLPTO with all the three sub-forces so far; see the references cited in Section I. In contrast, the force $f_{ei}(t) = f_{pto}(t)$ in (10) is generated completely during energy conversion by the energy conversion device comprising the PMLG and RLC network. It is entirely passive without external power injection (without negative power flow) and any additional mechanical devices. Hence, it can be physically and easily implemented. As far as we are aware of, (14) and (16)-(17) are the first of their kind that analytically describes the closed loop hydrodynamics of a whole WEC system, with the PTO feedback gains, M_{ei} , B_{ei} and K_{ei} , completely determined by the physical parameters of the PMLG and RLC , and with the force $f_{pto}(t) = f_C(t) + f_R(t) + f_L(t)$ generated fully internally within the WEC.

III. ELECTRIC OUTPUT POWER MAXIMIZATION

Applying the inverse Fourier transform to (16)-(17), it can be readily shown that for $f_w(t) = A_w \cos(\omega t)$ as given in (2), the (steady state) output of system (14) is given by

$$x(t) = |H(j\omega)|A_w \cos(\omega t + \varphi), \quad (18)$$

$$|H(j\omega)| = \frac{1}{|(K_m + K_{ei}) - \omega^2(M_m + M_{ei}) + j\omega(B_m + B_{ei})|}, \quad (19)$$

$$\varphi = \tan^{-1} \left(\frac{-\omega(B_m + B_{ei})}{(K_m + K_{ei}) - \omega^2(M_m + M_{ei})} \right), \quad (20)$$

where $|H(j\omega)|$ and φ are respectively the magnitude and phase of $H(j\omega)$. It then follows from (18) and $-\sin(\omega t + \varphi) = \cos(\omega t + \pi/2 + \varphi)$ that

$$\dot{x}(t) = \omega |H(j\omega)|A_w \cos(\omega t + \pi/2 + \varphi), \quad (21)$$

$$\ddot{x}(t) = -\omega^2 |H(j\omega)|A_w \cos(\omega t + \varphi). \quad (22)$$

As seen from (6)-(8) and (18)-(22), the amplitudes of internal voltage $v(t)$, current $i(t)$ and the instantaneous electric power $p(t) = v(t)i(t)$ are all maximized when the amplitude of $x(t)$, $|H(j\omega)|A_w$, is maximized. Therefore, maximizing $|H(j\omega)|$ maximizes the amplitude of $x(t)$, which in turn maximizes the amplitude of electric power $p(t)$.

A. Maximizing $|H(j\omega)|$ by LC tuning

As seen from (19), $|H(j\omega)|$ is maximized when its denominator $|(K_m + K_{ei}) - \omega^2(M_m + M_{ei}) + j\omega(B_m + B_{ei})| = \{[(K_m + K_{ei}) - \omega^2(M_m + M_{ei})]^2 + [\omega(B_m + B_{ei})]^2\}^{1/2}$ is minimized. From (3) and (9), $B_m > 0$ and $B_{ei} > 0$ for all $0 < R < \infty$. Hence, $[\omega(B_m + B_{ei})]^2 > [\omega B_m]^2 > 0$ always holds as long as there is an electric load $0 < R < \infty$. The only means to minimize $|H(j\omega)|$ under a given $0 < R < \infty$ is to tune K_{ei} and M_{ei} through L and C such that, ideally, $(K_m + K_{ei}) - \omega^2(M_m + M_{ei}) = 0$, or equivalently

$$\sqrt{(K_m + K_{ei})/(M_m + M_{ei})} = \omega. \quad (23)$$

When (23) is satisfied, $H(j\omega) = \frac{1}{j\omega(B_m + B_{ei})}$, which is purely imaginary with phase $\varphi = -\pi/2$ and maximum magnitude

$$|H(j\omega)| = |H(j\omega)|_{max} := \frac{1}{\omega(B_m + B_{ei})}, \quad (24)$$

and the system (14) resonates with its input force $f_w(t) = A_w \cos(\omega t)$; the amplitudes of $x(t)$, $\dot{x}(t)$, $\ddot{x}(t)$, $v(t)$, $i(t)$ and $p(t)$ are all maximized for the given electric load R .

When C and L are disconnected, $C = 0$, $L = \infty$, $M_{ei} = 0$, $K_{ei} = 0$, and (23) reduces to

$$\sqrt{K_m/M_m} = \omega_0. \quad (25)$$

This ω_0 is the natural frequency (or undamped resonant frequency) of conventional WECs studied in most of the previous, mechanically-focused, literature [1]. It is determined by the WECs' inherent mass M_m and stiffness K_m . Although, as noted in Section I, many ingenious mechanical techniques have been proposed to actively tune K_m or M_m [4], the vulnerability of complex mechanical linkages, valves or other devices needed for mechanical tuning has meant that in practice, to the best of our knowledge, K_m and M_m have

effectively been fixed for a conventional WEC. When $\omega \neq \omega_0$ due to changes in wave frequency, the conventional WEC will lose resonance, resulting in lower amplitudes of $x(t)$, $\dot{x}(t)$, $\ddot{x}(t)$, $e(t)$, $i(t)$ and $p(t)$.

Since M_{ei} and K_{ei} (defined in (9)) can be varied by varying C and L , the proposed WEC system can be tuned using C and L by the following three Rules derived from (23) and (25).

- 1) When $\omega = \omega_0$, disconnect C and L to make $C = 0$ and $L = \infty$ in (9) and hence $M_{ei} = 0$ and $K_{ei} = 0$ in (23).
- 2) When $\omega < \omega_0$, disconnect L to make $K_{ei} = 0$ and tune C to make $M_{ei} = K_m/\omega^2 - M_m$ in (23). From (9), the C (in Farad, F) thus tuned is given by

$$C = \frac{M_{ei}}{K_t K_e} = \frac{K_m/\omega^2 - M_m}{K_t K_e} > 0. \quad (26)$$

- 3) When $\omega > \omega_0$, disconnect C to make $M_{ei} = 0$ and tune L to make $K_{ei} = \omega^2 M_m - K_m$ in (23). From (9), the L (in Henry, H) thus tuned is given by

$$L = \frac{K_t K_e}{K_{ei}} = \frac{K_t K_e}{\omega^2 M_m - K_m} > 0. \quad (27)$$

These three Rules yield the same $H(j\omega)$ with $|H(j\omega)| = |H(j\omega)|_{max} = \frac{1}{\omega(B_m + B_{ei})}$ and phase $\varphi = -\pi/2$ for all $\omega > 0$. It then follows from (21) that under Rules 1)–3)

$$\dot{x}(t) \equiv \frac{A_w}{B_m + B_{ei}} \cos(\omega t), \forall \omega > 0, \quad (28)$$

which is in phase with $f_w(t) = A_w \cos(\omega t)$, $\forall \omega > 0$ and gives the instantaneous mechanical absorption of WEC

$$p_a(t) := f_w(t)\dot{x}(t) = \frac{A_w^2}{B_m + B_{ei}} \cos^2(\omega t) \geq 0, \forall t. \quad (29)$$

Therefore, the system (14) always resonates with the input force $f_w(t)$ and the amplitudes of $x(t)$, $\dot{x}(t)$, $\ddot{x}(t)$, $v(t)$, $i(t)$ and $p(t)$ are always maximized for the given electric load R , irrespective of the wave frequency ω .

It can be seen from (11)-(13), (18), (21), (22) and (28) that with Rules 1)–3), $f_R(t) = B_{ei}\dot{x}(t)$ is in phase with $f_w(t)$; $f_C(t) = M_{ei}\ddot{x}(t)$ leads and $f_L(t) = K_{ei}x(t)$ lags $f_w(t)$ by $\pi/2$ rad. As shown in III-B, only $f_R(t)$ absorbs average mechanical power. Hence, they are respectively the active, reactive leading and reactive lagging PTO sub-forces. They together produce the active and reactive PTO forces for different wave frequencies under Rules 1)–3), as shown in III-C. Moreover, from (26) and (27), the lower the $\omega < \omega_0$, the larger the C is required; and the higher the $\omega > \omega_0$, the smaller the L is required.

B. Maximizing mechanical power absorption by optimal R

From (14), the average mechanical power absorption P_a of the resonating WEC, over a full period T of $f_w(t)$, can be

written as

$$\begin{aligned}
P_a &= \frac{1}{T} \int_T p_a(t) dt = \frac{1}{T} \int_T f_w(t) \dot{x}(t) dt \\
&= \frac{1}{T} \int_T [M_m \ddot{x}(t) + B_m \dot{x}(t) + K_m x(t)] \dot{x}(t) dt + \\
&\quad \frac{1}{T} \int_T [M_{ei} \ddot{x}(t) + B_{ei} \dot{x}(t) + K_{ei} x(t)] \dot{x}(t) dt \quad (30) \\
&= \frac{B_m}{T} \int_T \dot{x}^2(t) dt + \frac{B_{ei}}{T} \int_T \dot{x}^2(t) dt \quad (31) \\
&= \frac{A_w^2 B_m}{2(B_m + B_{ei})^2} + \frac{A_w^2 B_{ei}}{2(B_m + B_{ei})^2} \quad (32) \\
&=: P_m + P_{ei}. \quad (33)
\end{aligned}$$

In the above, (31) follows from (18), (21) and (22) which show that $\ddot{x}(t)$ and $x(t)$ are orthogonal to $\dot{x}(t)$, when the WEC resonates at the frequency ω with $\varphi = -\pi/2$, and hence the first and third terms in the two integrals of (30) integrate to zero; (32) follows from substituting (28) into (31) and using $\cos^2(\omega t) = 1/2 + \cos(2\omega t)/2$.

As seen from (30)-(33), P_{ei} and P_m are the average mechanical powers absorbed by WEC through the PMLG induced damping force $B_{ei}\dot{x}(t)$ and the wave induced damping (radiation) force $B_m\dot{x}(t)$. Here B_m is the unchangeable inherent mechanical damping of WEC, while $B_{ei} = K_t K_e / R$ can be tuned using R to maximize P_m , P_{ei} and hence P_a .

Taking $dP_{ei}/dB_{ei} = A_w^2 \frac{(B_m + B_{ei}) - 2B_{ei}}{2(B_m + B_{ei})^3} = 0$ and solving for B_{ei} gives the optimal B_{ei} and the corresponding optimal electric load R , denoted as B_{ei}^* and R^* (in Ohm),

$$B_{ei}^* = B_m = K_t K_e / R^*, \quad R^* = K_t K_e / B_m, \quad (34)$$

and the resulting maximal average mechanical absorption P_{ei} , P_m and P_a , denoted as P_{ei}^* , P_m^* and P_a^* (in Watt), respectively.

$$P_{ei}^* = P_m^* = A_w^2 / 8B_m, \quad P_a^* = 2P_{ei}^* = 2P_m^* = A_w^2 / 4B_m. \quad (35)$$

Note that (34) and (35) hold for all $\omega > 0$ due to Rules 1)–3).

Remark 2: It is clear from (30) and (31) that the average mechanical power absorbed by the reactive sub-forces $(M_m + M_{ei})\ddot{x}(t)$ and $(K_m + K_{ei})x(t)$ is zero. This and the maximal average power absorption (35) are consistent with previous results, eg [1], [2], [14], but they now hold for all $\omega > 0$, instead of $\omega = \omega_0$ only, due to Rules 1)–3). The optimal electric load R^* and its maximal average power absorption P_{ei}^* are the first of their kind to the best of our knowledge.

C. Electric active power generated and reactive power needed

From (6) and (28), the output voltage $v(t)$ under Rules 1)–3) has the same amplitude as given below for all $\omega > 0$.

$$v(t) = K_e \dot{x}(t) = \frac{K_e A_w}{B_m + B_{ei}} \cos(\omega t) = \sqrt{2}V \cos(\omega t), \quad (36)$$

where $V = \sqrt{\frac{1}{T} \int_T v^2(t) dt} = K_e A_w / \sqrt{2}(B_m + B_{ei})$, in Volt, is the root mean square (RMS) of $v(t)$. It then follows from basic AC circuit analysis [32] that the current $i(t)$ is given by

$$i(t) = \sqrt{2}I \cos(\omega t + \psi), \quad (37)$$

where $I = V \sqrt{(1/R)^2 + (\omega C - 1/\omega L)^2}$, in Ampere, is the RMS of $i(t)$ and ψ is the phase of $i(t)$ vs $v(t)$ given by

$$\begin{aligned}
\psi &= \tan^{-1}[(\omega C - 1/\omega L)/(1/R)] \\
&= \cos^{-1}\left((1/R)/\sqrt{(1/R)^2 + (\omega C - 1/\omega L)^2}\right) \quad (38)
\end{aligned}$$

The instantaneous electric power can therefore be written as

$$\begin{aligned}
p(t) &= v(t)i(t) = 2VI \cos(\omega t) \cos(\omega t + \psi) \\
&= VI \cos(\psi) + VI \cos(2\omega t + \psi), \quad (39)
\end{aligned}$$

and the average electric output power can be written as

$$\begin{aligned}
P &= \frac{1}{T} \int_T p(t) dt = \frac{1}{T} \int_T VI [\cos(\psi) + \cos(2\omega t + \psi)] dt \\
&= VI \cos(\psi) = S \cos(\psi), \quad (40)
\end{aligned}$$

where P (in Watt) and $S := VI$ (in VA) are respectively the active and apparent electric power outputs of the PMLG, and

$$\cos(\psi) = (1/R)/\sqrt{(1/R)^2 + (\omega C - 1/\omega L)^2} := PF, \quad (41)$$

derived from (38), is the power factor (PF) of the PMLG.

When $\omega = \omega_0$ and Rule 1) is used, $\psi = 0$, $i(t) = i_R(t) = v(t)/R$ is in phase with $v(t)$, and $PF = 1$. When $\omega < \omega_0$ and Rule 2) is used, $\psi > 0$, $i(t) = i_R(t) + i_C(t)$ leads $v(t)$, and $PF < 1$. When $\omega > \omega_0$ and Rule 3) is used, $\psi < 0$, $i(t) = i_R(t) + i_L(t)$ lags $v(t)$, and $PF < 1$. Recall that $v(t) = K_e \dot{x}(t)$ and $\dot{x}(t)$ is in phase with $f_w(t)$ as shown in (28). Hence, under Rule 1), $f_{pto}(t) = K_t i_R(t) = f_R(t)$ yields the active PTO force in phase with $f_w(t)$; under Rule 2), $f_{pto}(t) = K_t i_R(t) + K_t i_C(t) = f_R(t) + f_C(t)$ yields the reactive PTO force leading $f_w(t)$; under Rule 3), $f_{pto}(t) = K_t i_R(t) + K_t i_L(t) = f_R(t) + f_L(t)$ yields the reactive PTO force lagging $f_w(t)$.

With V , I and $\cos(\psi)$ defined respectively in (36), (37) and (41), the active electric power P can be rewritten as

$$\begin{aligned}
P &= VI \cos(\psi) = V^2 \cos(\psi) \sqrt{(1/R)^2 + (\omega C - 1/\omega L)^2} \\
&= V^2 / R = K_e^2 A_w^2 / 2R(B_m + B_{ei})^2, \quad (42)
\end{aligned}$$

which is dependent on R but independent of PF . This is because R , L and C are in parallel connection with the same voltage source $v(t)$ and only R absorbs the active power P .

From (6), (7), (39), (40) and $K_e = K_t$, it follows that for any $0 < R < \infty$, $p(t) = v(t)i(t) = (K_e/K_t) f_{ei}(t) \dot{x}(t) = f_{ei}(t) \dot{x}(t) = p_{ei}(t)$ and $P = \frac{1}{T} \int_T p(t) dt = \frac{1}{T} \int_T p_{ei}(t) dt = P_{ei}$. By (34), (35) and (42), when $R = R^* = K_t K_e / B_m$, $P_{ei} = P_{ei}^* = A_w^2 / 8B_m$ for all $\omega > 0$, which is the maximal average mechanical power the PMLG can absorb. Hence, when the electric load $R = R^*$, the maximal active electric power output $P^* = P_{ei}^* = A_w^2 / 8B_m$ W is attained for all $\omega > 0$.

Although P is independent of PF , the apparent power $S = VI = P/PF$ does increase as PF decreases. Physically, PF decreases when ωC or $1/\omega L$ increases, which increases $i_C(t)$ or $i_L(t)$ and hence $i(t) = i_R(t) + i_L(t) + i_C(t)$ and its RMS (aka effective) value $I = V \sqrt{(1/R)^2 + (\omega C - 1/\omega L)^2}$. The increased $i(t)$ in turn increases the instantaneous PTO force $f_{pto}(t) = K_t i(t)$ and the effective PTO force $F_{pto} = K_t I$ to keep resonance at the frequency $\omega \neq \omega_0$. Consequently, the reactive power output, given by $Q = S \sin(\psi)$ (in VAR),

increases. When PF is low, the efficiency of the PMLG in active electric power generation becomes low. For the same level of P output, the PMLG's capacity rating $S = VI$ must be higher at lower PF since I flowing through the PMLG is higher. Therefore, to attain resonance and hence maximal active electric power output over a wider range of wave frequencies, we must use a PMLG with higher capacity (VA) rating to withstand higher I , and capacitor C with larger capacitance to provide higher I . This is the price we have to pay.

IV. SIMULATION STUDIES

Simulation studies are conducted to verify the proposed WEC and Tuning Rules 1)–3) and compare with the WEC without LC tuning. Simulations are performed using continuous-time dynamic system modules and the `ode15s` solver of MATLAB/Simulink with a time step of 0.01 seconds. The simulated WEC, having a buoy of radius $b_r = 1.5$ m and height $b_h = 2.75$ m, is adopted from [33] with $M_m = 10,000$ kg, $B_m = 4,000$ Ns/m, $K_m = 31,580$ N/m, $\omega_0 = \sqrt{K_m/B_m} = 1.77$ rad/s, $K_e = 842$ Vs/m, $K_t = 842$ N/A, and poles $N_p = 2$. The simulated wave input force $f_w(t) = A_w \cos(\omega t)$ has $A_w = 10$ kN and its frequency ω varied in the studies presented below.

From (34)–(35) and the analysis of Section III, the optimal electric resistor load for the simulated WEC is $R^* = K_e K_t / B_m = 177 \Omega$, which renders the maximum average mechanical power absorption $P_a^* = A_w^2 / 4B_m = 6.25$ kW and induces the maximum active electric output power $P^* = P_a^* / 2 = 3.125$ kW. Also, as given in (28), with $R = R^* = 177.5 \Omega$ and Rules 1)–3), the velocity of the WEC, $\dot{x}(t)$, is in phase with the input force $f_w(t)$ for all $\omega > 0$. Hence, we set $R = 177 \Omega$, and use these P_a^* and P^* values and $\dot{x}(t)$ in phase with $f_w(t)$ as the theoretical values and condition to check the simulation results in all the studies.

To facilitate comparison, we use blue curves to show the waveforms and superscript $*$ to represent the variables of tuned WEC, and use black curves for the waveforms of untuned WEC and red curves for the input force. The curves in Cases 1–3 are plotted from static start to steady state operation.

A. Case 1 ($\omega = \omega_0 = 1.77$ rad/s)

By Rule 1), the proposed WEC in this ideal case does not need tuning and the LC network is disconnected. Figs. 2–3 show the waveforms of the relevant variables of the WEC, which approach respective steady state amplitudes in about 7 s. As analyzed in Section III, the WEC resonates at the frequency $\omega = \omega_0 = 1.77$ rad/s, with its $\dot{x}(t)$ ($v(t) = K_e \dot{x}(t)$) and $f_{pto}(t)$ ($i(t) = f_{pto}(t) / K_t$) all in phase with $f_w(t)$; the amplitude of $f_{pto}(t)$ is well below that of $f_w(t)$; it absorbs the maximal mechanical power $P_a = P_a^* = 6.25$ kW, and the PMLG outputs the maximal active electric power $P = P^* = 3.125$ kW = P_{pto}^* , the maximal mechanical power it can absorb, with $PF = 1$. The PMLG capacity rating in this case must be $\geq S^* = P^* = 3.1255$ KVA.

B. Case 2 ($\omega = 1$ rad/s $< \omega_0 = 1.77$ rad/s)

By Rule 2), the proposed WEC in this case is tuned with $C = 0.0304$ F and L is disconnected. Figs. 4–5 show the

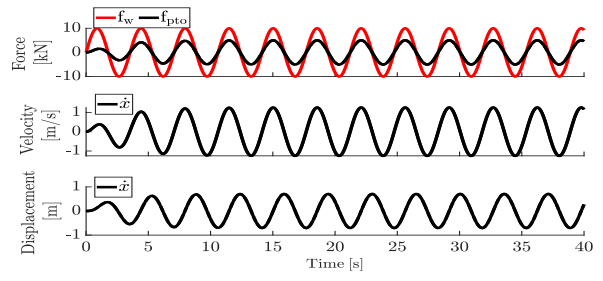


Fig. 2. WEC response at natural resonance frequency $\omega = \omega_0$

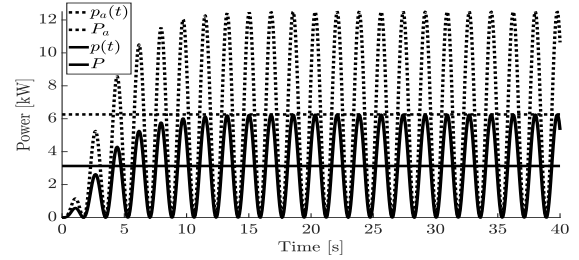


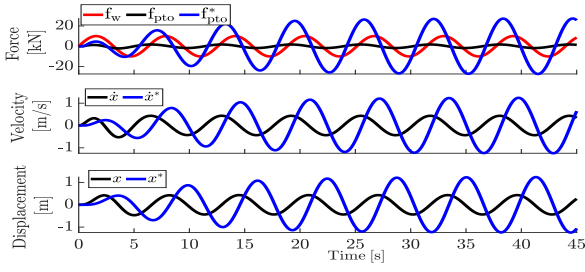
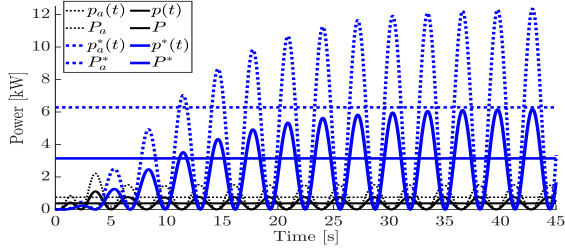
Fig. 3. Mechanical and active electrical powers of WEC at $\omega = \omega_0$

waveforms of the relevant variables of tuned and untuned WECs. The tuned and untuned WECs both oscillate at the frequency of $f_w(t)$, $\omega = 1$ rad/s, and the tuned waveforms approach respective steady state amplitudes in about 30 s. Compared with those of Case 1, the steady state amplitudes of tuned waveforms are the same or higher, whereas those of untuned waveforms are much lower. This is because the untuned WEC is not resonating with $f_w(t)$. Hence, its average mechanical power absorption $P_a = 1$ kW and active electric power output $P = 0.5$ kW, as opposed to $P_a^* = 6.25$ kW and $P^* = 3.125$ kW of the tuned WEC.

For the untuned WEC, the phases of its $f_{pto}(t)$, $\dot{x}(t)$ and $x(t)$ lead their tuned counterparts. For the tuned WEC, the phases of its $\dot{x}^*(t)$ and $x^*(t)$ remain the same as those in Case 1, with $\dot{x}^*(t)$ still in phase with $f_w(t)$, but its $f_{pto}^*(t)$ is no longer in phase with $f_w(t)$ as was in Case 1, instead, it now leads $f_w(t)$. The tuning capacitor C introduces $i_C(t)$ into $i^*(t) = i_R(t) + i_C(t)$ to significantly boost the amplitudes of $i^*(t)$ and $f_{pto}^*(t) = K_t i^*(t)$ and makes $i^*(t)$ leading $v^*(t) = K_e \dot{x}^*(t)$ and $f_{pto}^*(t) = K_t i^*(t)$ leading $f_w(t)$ by $\psi = 1.3886$ rad. The amplitude of this reactive leading PTO force $f_{pto}^*(t)$ is about 2.2 times higher than $f_w(t)$ and 4 times higher than in Case 1, which forces the tuned WEC to resonate at $\omega = 1$ rad/s instead of $\omega_0 = 1.77$ rad/s and output the maximal active electric power $P^* = 3.125$ kW. This is at the cost of low $PF = \cos(\psi) = 0.18$ and high $S^* = P^* / PF = 17.25$ KVA of PMLG as analyzed in III-C. So the PMLG capacity rating must be ≥ 17.25 KVA in order to maintain the 3.125 kW maximal active electric power output, when the wave frequency $\omega = 1$ rad/s is about 44% lower than WEC's natural frequency $\omega_0 = 1.77$ rad/s.

C. Case 3 ($\omega = 2.3$ rad/s $> \omega_0 = 1.77$ rad/s)

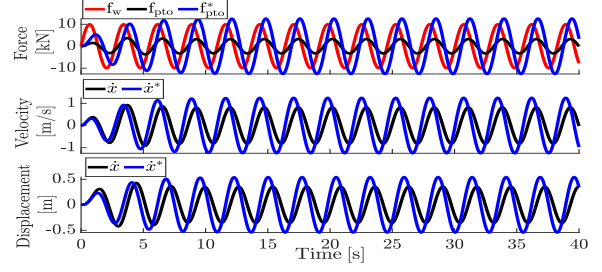
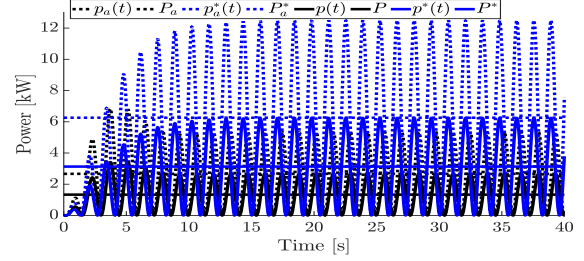
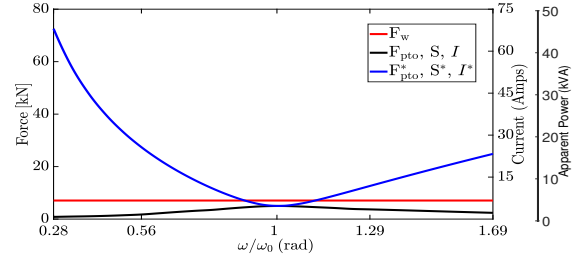
By Rule 3), the proposed WEC in this case is tuned with C disconnected and $L = 33.3113$ H. As seen from Figs. 6–7, similar to Case 2, both WECs oscillate at the


 Fig. 4. Responses of tuned and untuned WECs at $\omega < \omega_0$.

 Fig. 5. Mechanical and active electrical powers of tuned and untuned WECs at $\omega < \omega_0$

frequency of $f_w(t)$, $\omega = 2.3$ rad/s, and the tuned waveforms approach respective steady state amplitudes in about 12 s. The waveform amplitudes of the untuned WEC are significantly lower because it is not resonating with $f_w(t)$. Its average mechanical power absorption $P_a = 2.6$ kW and its active electric power output $P = 1.3$ kW, as opposed to $P_a^* = 6.25$ kW and $P^* = 3.125$ kW of tuned WEC. The phases of $f_{pto}(t)$, $\dot{x}(t)$ and $x(t)$ of the untuned WEC now lag their tuned counterparts. The phases of $\dot{x}^*(t)$ and $x^*(t)$ of the tuned WEC remain the same as those in Case 1, with $\dot{x}^*(t)$ still in phase with $f_w(t)$, but its $f_{pto}^*(t)$ now lags $f_w(t)$. The tuning inductor L introduces $i_L(t)$ into $i^*(t) = i_R(t) + i_L(t)$ to significantly boost the amplitudes of $i^*(t)$ and $f_{pto}^*(t) = K_t i^*(t)$ and make $i^*(t)$ lagging $v(t) = K_e \dot{x}^*(t)$ and $f_{pto}^*(t) = K_t i^*(t)$ lagging $f_w(t)$ by $\psi = 1.1674$ rad. The amplitude of this lagging reactive $f_{pto}^*(t)$ is about 20% higher than $f_w(t)$ and 2 times higher than in Case 1, which forces the tuned WEC to resonate at $\omega = 2.3$ rad/s, instead of $\omega_0 = 1.77$ rad/s, and output $P^* = 3.125$ kW. The cost for this is the low $PF = \cos(\psi) = 0.3925$ and high $S^* = P^*/PF = 7.92$ KVA of PMLG as analyzed in III-C. The PMLG capacity rating must be ≥ 7.92 KVA in order to maintain the 3.125 kW maximal active electric power output, when the wave frequency $\omega = 2.3$ rad/s is about 30% higher than WEC's natural frequency $\omega_0 = 1.77$ rad/s.

D. Case 4 ($0.5 \text{ rad/s} \leq \omega \leq 2.7 \text{ rad/s}$)

The proposed WEC in this case is tuned with Rules 1)-3) over $\omega \in [0.5, 2.7]$ rad/s and is compared with the untuned WECs over the same frequencies. Fig. 8 plots the effective input force F_w (RMS of $f_w(t)$), the RMS current I , effective PTO force $F_{pto} = K_t I$ and apparent power $S = VI$ of the PMLG in the tuned and untuned WECs over $\omega \in [0.5, 2.7]$, where I , F_{pto} and S share the same curves but with different scales since K_t and V are constants for all $\omega > 0$ as shown


 Fig. 6. Responses of tuned and untuned WECs at $\omega > \omega_0$.

 Fig. 7. Mechanical and active electrical powers of tuned and untuned WECs at $\omega > \omega_0$

 Fig. 8. RMS Currents I , effective PTO forces F_w and apparent powers S of PMLG in tuned and untuned WECs over $\omega \in [0.5, 2.7]$.

earlier. As seen from the plots, for the untuned WEC, its $F_{pto} < F_w, \forall \omega > 0$, and its I , F_{pto} and S fall off from the peak at $\omega = \omega_0$ when ω is above or below ω_0 (the black curve of Fig. 8), resulting in the decreased average mechanical power absorption P_a and active electric power output P (the black curves of Fig 9). In contrast, for the tuned WEC, its F_{pto}^* increases as ω shifts away from ω_0 and becomes significantly higher than F_w when ω is significantly lower or higher than ω_0 (the blue curve of Fig 8); this increased F_{pto}^* drives the tuned WEC to resonate with the input force at all $\omega > 0$ with significantly large I^* and S^* , and keeps its average mechanical power absorption P_a^* and active electric power output P^* constant for all $\omega > 0$ (the blue lines of Fig 9). As shown by the two example blue curves in Fig 9, Rules 1)-3) effectively shift the power curve as the input force frequency changes and align the power peak with the input force frequency ω . The apparent power S^* shown by the blue curve of Fig. 8 gives the lower bound for the PMLG capacity rating required at different wave frequencies.

V. DISCUSSIONS

Except for complicating the derivation and analysis, the neglected internal resistance R_{in} and inductance L_{in} of the PMLG do not affect the main results given above. The L_{in} yields some lagging in $i(t)$ and $f_{pto}(t) = K_t i(t)$, which can be easily compensated for by increasing the value of C if needed;

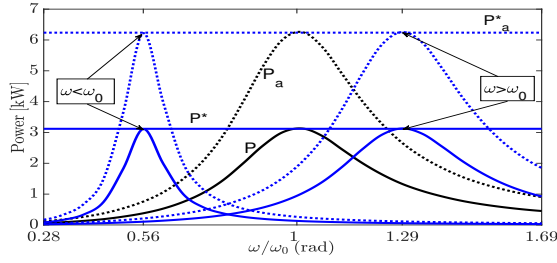


Fig. 9. Active powers vs wave frequency of tuned (blue) and untuned (black) WECs

R_{in} consumes some active electric power and reduces the net active electric power output of the PMLG, which is inevitable in all generators.

As shown analytically and experimentally in Sections III–IV, the capacity of the PMLG must be $\geq S^* = P^*/PF$ VA, where $P^* = A_w^*/8B_m W$, given in (35), is the maximal active electric power the WEC can produce, and $0 < PF < 1$ depends on the frequency range of $f_w(t)$ over which we want WEC to resonate. The leading (lagging) current $i_C(t)$ ($i_L(t)$) from C (L) and the corresponding reactive leading (lagging) $f_{pto}(t)$ are the key to the resonance at $\omega \neq \omega_0$. Limiting $i_C(t)$ ($i_L(t)$) will limit the frequency range of resonance or the oscillation amplitude of the WEC at $\omega \neq \omega_0$, leading to reduced electric power generation. Although these results are obtained for steady state operation of WEC without dynamic PTO control, they reveal a fundamental fact in the dynamic PTO control considered in many previous works, e.g. [12], [14], [18], [19]. The fact is that the leading and lagging reactive PTO forces are indispensable for the transient operation and control of WEC at $\omega \neq \omega_0$. Physically, the reactive PTO force can be easily induced in the generator by the L and C devices as shown above and controlled by controlling $i_C(t)$ and $i_L(t)$. However, this has not drawn much attention in the current literature.

The presented results are limited to the single-phase 2-pole PMLG, single frequency sinusoidal ocean wave, and steady state operation of WEC. Their extensions to multi-phase multi-pole linear and rotary generators, multi-frequency and broadband waves, and transient operation and control of WEC are currently being investigated.

VI. CONCLUSION

This paper has presented a novel LC -tuned WEC and its complete closed loop system model. Three quantitative rules have been derived from the closed loop system model to tune the reactive PTO forces produced by the LC device, for the WEC to resonate at $\omega \neq \omega_0$ and hence generate maximal electric power from ocean waves with variable frequency. Mathematical analysis of the WEC and tuning rules has led to the analytical and quantitative descriptions of the WEC's mechanical power absorption, active and reactive electric power generation and power factor, optimal electric load R , and capacity requirements of the PMLG and LC device. Simulation results have shown the effectiveness and advantages of the new WEC and verified the analysis results. The implications, limitations, and further extensions of the presented results have been discussed.

REFERENCES

- [1] Richard Manasseh. *Fluid Waves*. CRC Press, 2021.
- [2] John V Ringwood, Giorgio Bacelli, and Francesco Fusco. Energy-maximizing control of wave-energy converters: The development of control system technology to optimize their operation. *IEEE control systems magazine*, 34(5):30–55, 2014.
- [3] Umesh A Korde and John Ringwood. *Hydrodynamic control of wave energy devices*. Cambridge University Press, 2016.
- [4] Liguang Wang, Jan Isberg, and Elisabetta Tedeschi. Review of control strategies for wave energy conversion systems and their validation: the wave-to-wire approach. *Renewable and Sustainable Energy Reviews*, 81:366–379, 2018.
- [5] David IM Forehand, Aristides E Kiprakis, Anup J Nambiar, and A Robin Wallace. A fully coupled wave-to-wire model of an array of wave energy converters. *IEEE Transactions on Sustainable Energy*, 7(1):118–128, 2015.
- [6] Romain Genest, Félicien Bonnefoy, Alain H Clément, and Aurélien Babarit. Effect of non-ideal power take-off on the energy absorption of a reactively controlled one degree of freedom wave energy converter. *Applied Ocean Research*, 48:236–243, 2014.
- [7] Mohammad A Khasawneh and Mohammed F Daqaq. Internally-resonant broadband point wave energy absorber. *Energy Conversion and Management*, 247:114751, 2021.
- [8] Keita Sugiura, Ryoko Sawada, Yudai Nemoto, Ruriko Haraguchi, and Takehiko Asai. Wave flume testing of an oscillating-body wave energy converter with a tuned inerter. *Applied Ocean Research*, 98:102127, 2020.
- [9] JCC Henriques, LMC Gato, AF de O Falcao, Eider Robles, and F-X Fay. Latching control of a floating oscillating-water-column wave energy converter. *Renewable Energy*, 90:229–241, 2016.
- [10] Aurélien Babarit, Bruno Borgarino, Pierre Ferrant, and Alain Clément. Assessment of the influence of the distance between two wave energy converters on energy production. *IET renewable power generation*, 4(6):592–601, 2010.
- [11] Yifeng Gu, Boyin Ding, Nataliia Y Sergiienko, and Benjamin S Cazzolato. Power maximising control of a heaving point absorber wave energy converter. *IET Renewable Power Generation*, 15(14):3296–3308, 2021.
- [12] Uzair Bin Tahir, Jingxin Zhang, and Richard Manasseh. Latching control of wave energy converters using tunable electrical load. In *International Conference on Offshore Mechanics and Arctic Engineering*, volume 86908, page V008T09A073. American Society of Mechanical Engineers, 2023.
- [13] Bingyong Guo, Ron Patton, Mustafa Abdelrahman, and Jianglin Lan. A continuous control approach to point absorber wave energy conversion. In *2016 UKACC 11th International Conference on Control (CONTROL)*, pages 1–6. IEEE, 2016.
- [14] Joon Sung Park, Bon-Gwan Gu, Jeong Rok Kim, Il Hyoung Cho, Ilsu Jeong, and Ju Lee. Active phase control for maximum power point tracking of a linear wave generator. *IEEE transactions on power electronics*, 32(10):7651–7662, 2016.
- [15] Elisabetta Tedeschi, Matteo Carraro, Marta Molinas, and Paolo Mattavelli. Effect of control strategies and power take-off efficiency on the power capture from sea waves. *IEEE Transactions on Energy Conversion*, 26(4):1088–1098, 2011.
- [16] P Hardy, BS Cazzolato, B Ding, and Z Prime. A maximum capture width tracking controller for ocean wave energy converters in irregular waves. *Ocean Engineering*, 121:516–529, 2016.
- [17] Jianan Xu, Yanpeng Zhao, Yong Zhan, and Yansong Yang. Maximum power point tracking control for mechanical rectification wave energy converter. *IET Renewable Power Generation*, 15(14):3138–3150, 2021.
- [18] Nataliia Y Sergiienko, Giorgio Bacelli, Ryan G Coe, and Benjamin S Cazzolato. A comparison of efficiency-aware model-predictive control approaches for wave energy devices. *Journal of Ocean Engineering and Marine Energy*, 8(1):17–29, 2022.
- [19] Jitendra K Jain, Oliver Mason, Hafiz A Said, and John V Ringwood. Limiting reactive power flow peaks in wave energy systems. *IFAC-PapersOnLine*, 55(31):427–432, 2022.
- [20] Abdus Samad, SA Sannasiraj, Vallam Sundar, and Paresh Halder. *Ocean Wave Energy Systems: Hydrodynamics, Power Takeoff and Control Systems*. Springer, 2022.
- [21] Markel Penalba and John V Ringwood. A review of wave-to-wire models for wave energy converters. *Energies*, 9(7):506, 2016.
- [22] Erwin WJ Bergsma, Rafael Almar, Edward J Anthony, Thierry Garlan, and Elodie Kestenare. Wave variability along the world's continental shelves and coasts: Monitoring opportunities from satellite earth observation. *Advances in Space Research*, 69(9):3236–3244, 2022.

- [23] Hafiz Ahsan Said, Demián García-Violini, and John V Ringwood. Wave-to-grid (w2g) control of a wave energy converter. *Energy Conversion and Management: X*, 14:100190, 2022.
- [24] K. Budal. Theory for absorption of wave power by a system of interacting bodies. *J. Ship Res.*, 21(4):248–253, 1977.
- [25] Ye Li and Yi-Hsiang Yu. A synthesis of numerical methods for modeling wave energy converter-point absorbers. *Renewable and Sustainable Energy Reviews*, 16(6):4352–4364, 2012.
- [26] Antonio F de O Falcao. Wave energy utilization: A review of the technologies. *Renewable and sustainable energy reviews*, 14(3):899–918, 2010.
- [27] WE Cummins et al. The impulse response function and ship motions. 1962.
- [28] Apram Raheer. Comparison of control strategies for wave energy converters, 2020.
- [29] Yifan Song. *Design and Fabrication of a Linear Generator for Hybrid Systems*. North Carolina State University, 2019.
- [30] Peter F Ryff. *Electric machinery*. Prentice Hall, 1994.
- [31] Huibert Kwakernaak. *Modern signals and systems*. Prentice Hall, 1991.
- [32] James William Nilsson. *Electric circuits*. Pearson Education, 2008.
- [33] Marios Charilaos Sousounis, Leong Kit Gan, Aristides E Kiprakis, and Jonathan KH Shek. Direct drive wave energy array with offshore energy storage supplying off-grid residential load. *IET Renewable Power Generation*, 11(9):1081–1088, 2017.